

# Phase Asymmetry and Fractional-Order TV Ultrasound Speckle Filtering

Kunming He, Binjie Qin<sup>1</sup>, Member, IEEE

**Abstract**—We propose an ultrasound speckle filtering method for not only preserving various edge features but also filtering tissue-dependent complex speckle noises in ultrasound images. The key idea is to detect these various edges using a phase congruence-based edge significance measure called phase asymmetry (PAS), which is invariant to the intensity amplitude of edges and takes 0 in non-edge smooth regions and 1 at the idea step edge, while also taking intermediate values at slowly varying ramp edges. By leveraging the PAS metric in designing weighting coefficients to maintain a balance between fractional-order anisotropic diffusion and total variation (TV) filters in TV cost function, we propose a new fractional TV framework to not only achieve the best despeckling performance with ramp edge preservation but also reduce the staircase effect produced by integral-order filters. Then, we exploit the PAS metric in designing a new fractional-order diffusion coefficient to properly preserve low-contrast edges in diffusion filtering. Finally, different from fixed fractional-order diffusion filters, an adaptive fractional order is introduced based on the PAS metric to enhance various weak edges in the spatially transitional areas between objects. The proposed fractional TV model is minimized using the gradient descent method to obtain the final denoised image. The experimental results and real application of ultrasound breast image segmentation show that the proposed method outperforms other state-of-the-art ultrasound despeckling filters for both speckle reduction and feature preservation in terms of visual evaluation and quantitative indices. The best scores on feature similarity indices have achieved 0.867, 0.844 and 0.834 under three different levels of noise, while the best breast ultrasound segmentation accuracy in terms of the mean and median dice similarity coefficient are 96.25% and 96.15%, respectively.

**Index Terms**—Ultrasound despeckling, speckle noise, fractional-order diffusion filter, fractional-order TV filter, edge detection, phase congruency, phase asymmetry, image denoising.

M. He received his M.S. degree in 2019, and his Ph.D. degree in 2020 from the School of Information Engineering, Beijing University of Aeronautics and Astronautics, Beijing, China. He is currently a postdoctoral research fellow with the School of Information Engineering, Beijing University of Aeronautics and Astronautics. His research interests include image denoising and edge detection.

B. Qin received his M.S. degree in 2019, and his Ph.D. degree in 2022 from the School of Information Engineering, Beijing University of Aeronautics and Astronautics, Beijing, China. He is currently an associate professor with the School of Information Engineering, Beijing University of Aeronautics and Astronautics. His research interests include image denoising and edge detection.

<sup>1</sup>Corresponding author: Binjie Qin (E-mail: qinbj@buaa.edu.cn).  
This work was supported by the National Natural Science Foundation of China (Grant 61271320).

Manuscript received October 10, 2019; revised February 10, 2020; accepted March 10, 2020. This work was supported by the National Natural Science Foundation of China (Grant 61271320).

## I. INTRODUCTION

Ultrasound speckle is a complex noise that is inherent in ultrasound images, which significantly affects the diagnosis and segmentation of medical images. To reduce the speckle noise, many methods have been proposed, such as non-local means (NLM) [1], [2], wavelet-based methods [3], [4], and total variation (TV) [5], [6]. However, these methods often suffer from the staircase effect and edge blurring. Recently, fractional-order methods have been proposed to address these issues. Fractional-order TV [7] and fractional-order diffusion [8] have been shown to be effective in preserving edges while reducing speckle. In this paper, we propose a new fractional TV framework that combines phase asymmetry (PAS) and fractional-order TV. The PAS metric is used to design weighting coefficients that balance the fractional-order TV and fractional-order diffusion. The proposed method not only achieves the best despeckling performance but also reduces the staircase effect. The experimental results show that the proposed method outperforms other state-of-the-art ultrasound despeckling filters for both speckle reduction and feature preservation in terms of visual evaluation and quantitative indices. The best scores on feature similarity indices have achieved 0.867, 0.844 and 0.834 under three different levels of noise, while the best breast ultrasound segmentation accuracy in terms of the mean and median dice similarity coefficient are 96.25% and 96.15%, respectively.

The rest of the paper is organized as follows. Section II describes the proposed fractional TV framework. Section III presents the experimental results and real application of ultrasound breast image segmentation. Section IV concludes the paper.

[15] I. F. ... C. F. *et al.* [16] ... M. ... (SBF) [17] ... H. ... T. NLM ... NLM ... C. *et al.* [18] ... B. ... NLM (OBNLM) ... G. ... A. ... OBNLM ... Z. *et al.* [19] ... R. ... Z. *et al.* [20] ... (NLLRF) ... H. ... NLM ... [21]. ... I. ... P. ... M. ... (AD) [22], ... (SRAD) [23] ... (DPAD) [24] ... T. SRAD ... DPAD ... T. [25] ... U. ... C. *et al.* [16] ... U. ... [26] ... H. ... [27] ... M. ... T. ... B. ... F. [28] ... N. ... AD (FAD) ... R. ... F. *et al.* [8] ... G. ... (ADLG) ... H. ... ADLG ... B. ... AD

[29] ... [30] ... AD ... H. ... E. ... T. ... A. ... [31]. ... T. ... [32] ... T. ... O. *et al.* [33] ... H. ... [2] ... C. *et al.* [34] ... S. ... [35], ... [36], ... [37], [38], ... H. ... T. ... [39], [40] ... I. ... M. ... M. *et al.* [41], [42]. ... F. ... A. ... T. ... M. ... T. ... M. ... P. ... N. [43]. W. ... (PC) ... [44] ... (PAS, ... (PS) ... T. ... D)

Acro

[REDACTED]



Fig. 2. The proposed PAS algorithm flowchart.

The proposed PAS algorithm flowchart is shown in Fig. 2. The input image  $I$  is first processed by the Fractional-Order AD Filter (FOAD) to produce the denoised image  $I_{AD}$ . The FOAD filter is based on the Fractional-Order Anisotropic Diffusion (FOAD) method [46]. The FOAD method is a generalization of the Anisotropic Diffusion (AD) method [47]. The AD method is a nonlinear diffusion process that smooths the image while preserving edges. The FOAD method introduces a fractional-order derivative to the AD method, which allows for more flexible control of the smoothing process. The FOAD method is defined by the following equation [46]:

$$\frac{\partial u}{\partial t} = \text{div} [c(|\nabla u|) \cdot \nabla u], \quad (8)$$

where  $u$  is the image intensity,  $t$  is the time,  $\text{div}$  is the divergence operator,  $c(\cdot)$  is the diffusion coefficient, and  $\nabla u$  is the gradient of  $u$ . The diffusion coefficient  $c(\cdot)$  is defined as:

$$c(\cdot) = \frac{1}{1 + |\nabla u|^\alpha}, \quad (9)$$

where  $\alpha$  is the fractional order. The FOAD method is implemented by the Fractional-Order AD Filter (FOAD) [46]. The FOAD filter is based on the Fractional-Order Anisotropic Diffusion (FOAD) method [46]. The FOAD method is a generalization of the Anisotropic Diffusion (AD) method [47]. The AD method is a nonlinear diffusion process that smooths the image while preserving edges. The FOAD method introduces a fractional-order derivative to the AD method, which allows for more flexible control of the smoothing process. The FOAD method is defined by the following equation [46]:

$$D^\alpha f(x) \triangleq \lim_{h \rightarrow 0} \frac{1}{h^\alpha} \sum_{l=0}^{[\frac{d-c}{h}]} (-1)^l \binom{\alpha}{l} f(x-lh) \quad (6)$$

where  $\alpha \in [c, d]$ ,  $[c, d]$  is the interval of the fractional order,  $f(x)$  is the function,  $\frac{d-c}{h} \in [\frac{d-c}{h}]$ , and  $\binom{\alpha}{l}$  is the binomial coefficient:

$$\binom{\alpha}{l} = \frac{\Gamma(\alpha+1)}{\Gamma(l+1)\Gamma(\alpha-l+1)} \quad (7)$$

where  $\Gamma(n) = (n-1)!$ .

C. Fractional-Order AD Filter and Fractional-Order TV Filter

The Fractional-Order AD Filter (FOAD) [22] is defined as:

$$\frac{\partial u}{\partial t} = \text{div} [c(|\nabla u|) \cdot \nabla u], \quad (8)$$

where  $\text{div}$  is the divergence operator,  $c(\cdot)$  is the diffusion coefficient, and  $\nabla u$  is the gradient of  $u$ . The diffusion coefficient  $c(\cdot)$  is defined as:

$$c(\cdot) = \frac{1}{1 + |\nabla u|^\alpha}, \quad (9)$$

where  $\alpha$  is the fractional order.

where  $\lambda$  is the regularization parameter. The proposed method is compared with the state-of-the-art methods: FAD [60], WFTV [61], and PAS [62]. The PSNR and SSIM are used as the evaluation metrics. The results are shown in Table I. The proposed method achieves the highest PSNR and SSIM values, indicating that it can effectively remove the noise while preserving the image details.

$$\begin{cases} \varphi = (PA - 1)^2 \\ \gamma = PA(2 - PA) \end{cases} \quad (15)$$

where  $PA$  is the parameter of the proposed method. The proposed method is compared with the state-of-the-art methods: FAD [60], WFTV [61], and PAS [62]. The PSNR and SSIM are used as the evaluation metrics. The results are shown in Table I. The proposed method achieves the highest PSNR and SSIM values, indicating that it can effectively remove the noise while preserving the image details.

The proposed method is compared with the state-of-the-art methods: FAD [60], WFTV [61], and PAS [62]. The PSNR and SSIM are used as the evaluation metrics. The results are shown in Table I. The proposed method achieves the highest PSNR and SSIM values, indicating that it can effectively remove the noise while preserving the image details.

$$c(|\nabla^\alpha u|, PA) = 1 / \left[ 1 + \frac{|\nabla^\alpha u| \cdot (1 + 254 \cdot PA)}{k_1^2} \right] \quad (16)$$

where  $k_1 = k_0 e^{-0.05(n_{iter}-1)}$  and  $k_0$  is the initial value of  $k_1$ .

The proposed method is compared with the state-of-the-art methods: FAD [60], WFTV [61], and PAS [62]. The PSNR and SSIM are used as the evaluation metrics. The results are shown in Table I. The proposed method achieves the highest PSNR and SSIM values, indicating that it can effectively remove the noise while preserving the image details.

The proposed method is compared with the state-of-the-art methods: FAD [60], WFTV [61], and PAS [62]. The PSNR and SSIM are used as the evaluation metrics. The results are shown in Table I. The proposed method achieves the highest PSNR and SSIM values, indicating that it can effectively remove the noise while preserving the image details.

$$\alpha = 1 + \frac{1}{2} (1 + PA^2) \quad (17)$$

where  $PA \in (1, 2)$ . The proposed method is compared with the state-of-the-art methods: FAD [60], WFTV [61], and PAS [62]. The PSNR and SSIM are used as the evaluation metrics. The results are shown in Table I. The proposed method achieves the highest PSNR and SSIM values, indicating that it can effectively remove the noise while preserving the image details.

The proposed method is compared with the state-of-the-art methods: FAD [60], WFTV [61], and PAS [62]. The PSNR and SSIM are used as the evaluation metrics. The results are shown in Table I. The proposed method achieves the highest PSNR and SSIM values, indicating that it can effectively remove the noise while preserving the image details.

The proposed method is compared with the state-of-the-art methods: FAD [60], WFTV [61], and PAS [62]. The PSNR and SSIM are used as the evaluation metrics. The results are shown in Table I. The proposed method achieves the highest PSNR and SSIM values, indicating that it can effectively remove the noise while preserving the image details.

## B. Numerical Solver

The proposed method is compared with the state-of-the-art methods: FAD [60], WFTV [61], and PAS [62]. The PSNR and SSIM are used as the evaluation metrics. The results are shown in Table I. The proposed method achieves the highest PSNR and SSIM values, indicating that it can effectively remove the noise while preserving the image details.

$$\begin{aligned} \Phi(e) &:= E(u + e\eta) \\ &= \int_{\Omega} [\varphi f(|\nabla^\alpha(u + e\eta)|) + \gamma |\nabla^\alpha(u + e\eta)|] dx dy \\ &\quad + \int_{\Omega} \left( \frac{\lambda}{2} |u + e\eta - u_0|^2 \right) dx dy \end{aligned} \quad (18)$$

The proposed method is compared with the state-of-the-art methods: FAD [60], WFTV [61], and PAS [62]. The PSNR and SSIM are used as the evaluation metrics. The results are shown in Table I. The proposed method achieves the highest PSNR and SSIM values, indicating that it can effectively remove the noise while preserving the image details.

$$\begin{aligned} \Phi'(e) &= \frac{d}{de} \Phi(e) \\ &= \varphi \int_{\Omega} \left( f'(|\nabla^\alpha(u + e\eta)|) \right. \\ &\quad \times \left. \frac{\nabla_x^\alpha(u + e\eta) \nabla_x^\alpha \eta + \nabla_y^\alpha(u + e\eta) \nabla_y^\alpha \eta}{\sqrt{(\nabla_x^\alpha(u + e\eta))^2 + (\nabla_y^\alpha(u + e\eta))^2}} \right) dx dy \\ &\quad + \gamma \int_{\Omega} \left( \frac{\nabla_x^\alpha(u + e\eta) \nabla_x^\alpha \eta + \nabla_y^\alpha(u + e\eta) \nabla_y^\alpha \eta}{\sqrt{(\nabla_x^\alpha(u + e\eta))^2 + (\nabla_y^\alpha(u + e\eta))^2}} \right) dx dy \\ &\quad + \lambda \int_{\Omega} (u + e\eta - u_0) \eta dx dy, \end{aligned} \quad (19)$$

where  $e = 0$ , and  $\eta$  is the search direction.

$$\begin{aligned} \Phi'(0) &= \varphi \int_{\Omega} \left( c(|\nabla^\alpha u|^2, PA^2) (\nabla_x^\alpha u \nabla_x^\alpha \eta + \nabla_y^\alpha u \nabla_y^\alpha \eta) \right) dx dy \\ &\quad + \gamma \int_{\Omega} \frac{\nabla_x^\alpha u \nabla_x^\alpha \eta + \nabla_y^\alpha u \nabla_y^\alpha \eta}{|\nabla^\alpha u|} dx dy \\ &\quad + \lambda \int_{\Omega} (u - u_0) \eta dx dy \end{aligned} \quad (20)$$

where  $|\nabla^\alpha u| = \sqrt{(\nabla_x^\alpha u)^2 + (\nabla_y^\alpha u)^2}$ . The proposed method is compared with the state-of-the-art methods: FAD [60], WFTV [61], and PAS [62]. The PSNR and SSIM are used as the evaluation metrics. The results are shown in Table I. The proposed method achieves the highest PSNR and SSIM values, indicating that it can effectively remove the noise while preserving the image details.

$\Phi'(0) = 0$ . Then, by (20), we have

$$\nabla_x^\alpha u \nabla_x^\alpha \eta + \nabla_y^\alpha u \nabla_y^\alpha \eta = \left( (\nabla_x^\alpha)^* \nabla_x^\alpha u + (\nabla_y^\alpha)^* \nabla_y^\alpha u \right) \eta \quad (21)$$

By (62), we have

$$\begin{aligned} \Phi'(0) &= \varphi \int_{\Omega} c(|\nabla^\alpha u|^2, PA^2) \left( (\nabla_x^\alpha)^* \nabla_x^\alpha u + (\nabla_y^\alpha)^* \nabla_y^\alpha u \right) \eta \, dy \\ &\quad + \gamma \int_{\Omega} \frac{(\nabla_x^\alpha)^* \nabla_x^\alpha u + (\nabla_y^\alpha)^* \nabla_y^\alpha u}{|\nabla^\alpha u|} \eta \, dy \\ &\quad + \lambda \int_{\Omega} (u - u_0) \eta \, dy \end{aligned} \quad (22)$$

For  $\eta \in C^\infty(\Omega)$ , we have

$$\begin{aligned} \varphi c(|\nabla^\alpha u|^2, PA^2) \left( (\nabla_x^\alpha)^* \nabla_x^\alpha u + (\nabla_y^\alpha)^* \nabla_y^\alpha u \right) \\ + \gamma \frac{(\nabla_x^\alpha)^* \nabla_x^\alpha u + (\nabla_y^\alpha)^* \nabla_y^\alpha u}{|\nabla^\alpha u|} + \lambda(u - u_0) = 0 \end{aligned} \quad (23)$$

Let  $u$  be the solution of (23). Then, we have  $\nabla E(u) = 0$ . Then, we have

$$\begin{aligned} \nabla E = \varphi c(|\nabla^\alpha u|^2, PA^2) \left( (\nabla_x^\alpha)^* \nabla_x^\alpha u + (\nabla_y^\alpha)^* \nabla_y^\alpha u \right) \\ + \gamma \frac{(\nabla_x^\alpha)^* \nabla_x^\alpha u + (\nabla_y^\alpha)^* \nabla_y^\alpha u}{|\nabla^\alpha u|} + \lambda(u - u_0) \end{aligned} \quad (24)$$

By (63), we have

### C. Numerical Algorithm

Then, by (24), we have

$$\begin{cases} \nabla_x^\alpha u_{i,j} = \sum_{l=0}^j (-1)^l \binom{\alpha}{l} u_{i,j-l} \\ \nabla_y^\alpha u_{i,j} = \sum_{l=0}^i (-1)^l \binom{\alpha}{l} u_{i-l,j} \end{cases} \quad (25)$$

$$\begin{cases} (\nabla_x^\alpha)^* u_{i,j} = \sum_{l=0}^{Y-1-j} (-1)^l \binom{\alpha}{l} u_{i,j+l} \\ (\nabla_y^\alpha)^* u_{i,j} = \sum_{l=0}^{X-1-i} (-1)^l \binom{\alpha}{l} u_{i+l,j} \end{cases} \quad (26)$$

---

### Algorithm 1 PFDTV F -P -D -F

---

**Input:**

TABLE II  
COMPARISON OF THE PSNR, MSSIM AND FSIM VALUES AMONG DIFFERENT FILTERS

---







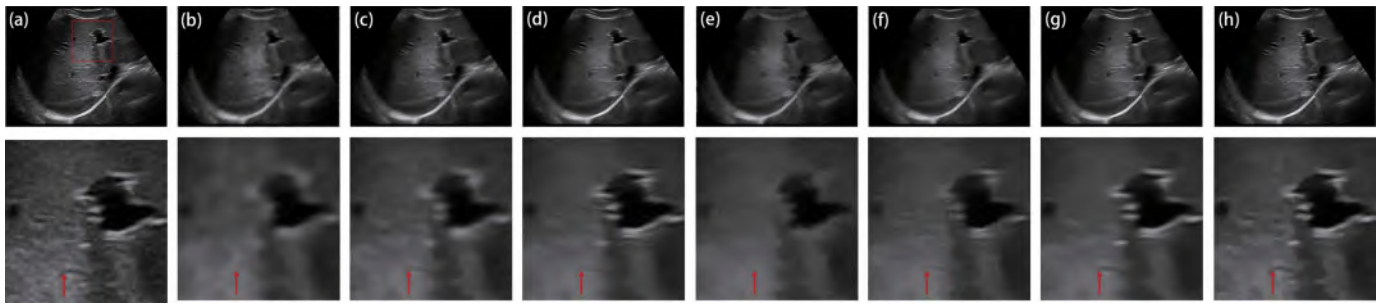


Fig. 6. Denoising results of the proposed method and other methods on the simulated data. (a)  $T_F$ , (b)  $F_{L1}$ , (c) SRAD, (d) OBNLM, (e) SBF, (f) ADLG, (g) NLLRF, (h) PFDTV.

Fig. 7. Denoising results of the proposed method and other methods on the real data. (a)  $T_F$ , (b)  $F_{L1}$ , (c)  $F_{L1}$ , (d) SRAD, (e) OBNLM, (f) SBF, (g) ADLG, (h) NLLRF, (i) PFDTV.

SRAD, OBNLM, NLLRF, ADLG, SBF,  $F_{L1}$ ,  $T_F$ , and PFDTV. The proposed method (PFDTV) shows superior performance in preserving edge information and reducing noise compared to other methods. The zoomed-in regions in Fig. 6 and Fig. 7 clearly demonstrate the effectiveness of the proposed method in handling both simulated and real data.

Tf

TABLE III

THE MEAN AND SD AND HM V  
SOME EXPERIMENTAL RESULTS  
OF THE PAS ULTRASOUND

	(%)
mp	
Fr	3.
	94
OBLEM	95.64 90.89 8.0608 1.

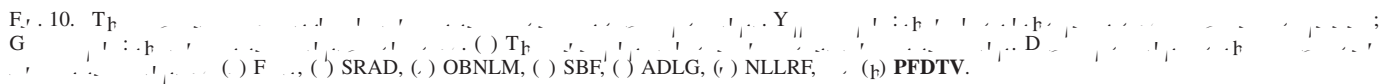


TABLE IV  
THE MEDIAN DSC, JS, HD AND HM VALUES FOR DIFFERENT  
SEGMENTATION RESULTS ON TEN BREAST  
ULTRASOUND IMAGES

---

[2], ACVA, P-G, [78], [79], PFDTV, [35], [76], [80], M, 3D, [7], [81], H, [82], T, [39], F, [38], [39], I, TV, FAD, FTV, S, TV

ACKNOWLEDGMENT

T

- [29] A. S. L., H. M. P., A. . . . *Measurement*, . 140, . 572-581, J. . 2019.
- [30] D. G., R. S. A., B. T., S. . . . *IET Image Process.*, . 9, . 2, . 107-117, 2015.
- [31] Z. Q., L. Y., W. L., A. . . . *Proc. BMVC*, 2011, . 73.
- [32] V. B. S. P., R. P., G. S., K. P., M. . . . *IEEE Trans. Image Process.*, . 28, . 12, . 6198-6210, D. . 2019.
- [33] N. O., M. G., S. A., A. B., B. N., R. B., O. . . . *IEEE Trans. Pattern Anal. Mach. Intell.*, . 10.1109/TPAMI.2019.2892134.
- [34] R. C., R. S., L. M., H. B., A. . . . *arXiv:1904.10235*. [O. . . .] A. . . . // . /1904.10235
- [35] V. K., A. F., K. E., J. A., F. . . . *Int. J. Comput. Vis.*, . 86, . 1, . 1-32, 2010.
- [36] H. T., S. F., P. M., K. . . . *IEEE Trans. Image Process.*, . 16, . 2, . 349-366, F. . 2007.
- [37] B. Q., Z. S., Z. Z., J. Z., Y. L., S. . . . *Appl. Soft Comput.*, . 46, . 851-867, S. . 2016.
- [38] B. Q., Z. S., Z. F., Z. Z., Y. L., J. B., J. . . . *IEEE Access*, . 6, . 1, . 330-343, 2018.
- [39] L. Z., W. W., J. Q., K.-H. W., K.-S. C., P.-A. H., F. . . . *Signal Process.*, . 134, . 275-284, M. . 2017.
- [40] A. B., D. B., Y. M., P. . . . *IEEE Trans. Inf. Technol. Biomed.*, . 15, . 1, . 138-147, J. . 2011.
- [41] M. C. M., J. R., D. C. B., R. O., M. . . . *Nature*, . 324, . 6049, . 250-253, N. . 1986.
- [42] M. C. M., R. A. O., F. . . . *Pattern Recognit. Lett.*, . 6, . 5, . 303-313, D. . 1987.
- [43] M. M., P., J. A. N., 2D+T . . . . *Med. Image Anal.*, . 4, . 1, . 21-30, 2000.
- [44] P. K., I. . . . *J. Comput. Vis. Res.*, . 1, . 3, . 1-26, 1999.
- [45] G.-Q. Z., W.-W. J., K.-L. L., Y.-P. Z., A. . . . 3-D . . . . *IEEE Trans. Med. Imag.*, . 36, . 6, . 1250-1262, J. . 2017.
- [46] Q. Z., J. G., Z. W., K. L., A. . . . *IEEE Trans. Geosci. Remote Sens.*, . 54, . 4, . 1905-1917, A. . 2016.
- [47] J. Y., L. T., S. Z., L. W., M. A. S., I. . . . *IEEE Access*, . 5, . 12275-12285, 2017.
- [48] V. M., P. R., M. S. P., M. . . . AM-FM . . . . *IEEE Trans. Image Process.*, . 19, . 5, . 1138-1152, M. . 2010.
- [49] J. P. H., P. T., A. C. B., AM-FM . . . . *Handbook of Image and Video Processing*. A. . . . T. N. . . . : E. . . . 2005, . 377-395.
- [50] M. C., T. O., V. P., T. . . . A. . . . T. . . . 1.6(-)-364.7784-1.8(-)-3.4(-16.0057-2.2647TD-0.0045T 2[( . . .)-AM95.75.366 4-10.2()2.7(-)-1.474.9(67.6(-)]TJ/F21T 2.2888

[76] B. G. et al., A. D. et al., S. A. et al., B. S. S. et al., A. S. et al., I. et al., *Fusion*, vol. 55, pp. 220–244, Mar. 2020.

[77] C. A. N. S. et al., N. D. A. M. et al., G. et al., *IEEE Trans. Image Process.*, vol. 28, pp. 216–226, Jan. 2019.

[78] Y. J. et al., X. J. et al., W. J. et al., A. et al., *J. Vis. Commun. Image Represent.*, vol. 65, Dec. 2019, Art. ID. 102661, doi: 10.1016/j.jvcir.2019.102661.

[79] Y.-F. P. et al., A. et al., *IEEE Trans. Image Process.*, vol. 27, pp. 1214–1229, Mar. 2018.

[80] F. Z. et al., R. et al., P. et al., X. et al., *Phys. Med. Biol.*, vol. 58, pp. 1739, 2013.

[81] R. J. G. et al., S. et al., R. C. et al., Y. C. E. et al., D. et al., *Proc. IEEE*, pp. 10.1109/JPROC.2019.2932116.

[82] X. J. et al., S. L. et al., X. F. et al., L. Z. et al., FOCN: A *Proc. IEEE Conf. Comput. Vis. Pattern Recognit.*, pp. 6054–6063, 2019.



**Kunqiang Mei** received B.S. degree from Anhui University, Anhui, China, in 2016, M.S. degree from Jilin University, Jilin, China, in 2019, and Ph.D. degree from Jilin University, Jilin, China, in 2021. He is currently an associate professor at Jilin University. His research interests include image denoising, image inpainting, and image segmentation.



**Bin Hu** received M.S. degree from Tianjin University, Tianjin, China, in 1997, and M.D.-Ph.D. degree from Jilin University, Jilin, China, in 2006. He is currently an associate professor at Jilin University. His research interests include image denoising, image inpainting, and image segmentation.



**Baowei Fei** received M.S. and Ph.D. degrees from Case Western Reserve University, Cleveland, OH, USA, in 1995 and 1998, respectively. He is currently an associate professor at Jilin University, Jilin, China. His research interests include image denoising, image inpainting, and image segmentation.



**Binjie Qin (M'07)** received M.S. degree from Nanjing University, Nanjing, China, in 1999, and Ph.D. degree from Jilin University, Jilin, China, in 2002. He is currently an associate professor at Jilin University. His research interests include image denoising, image inpainting, and image segmentation.